Multi-sinusoidal Disturbance Rejection for Uncertain Discrete-Time Linear Systems

Jiangkun Xu, Yizhou Gong, Yang Wang *Member, IEEE*

***Abstract*— This paper proposes a novel adaptive feedforward control (AFC)-based regulator for disturbance rejection in highly uncertain discrete-time linear systems. The focus is on addressing the challenges arising from biased multi-sinusoidal disturbances characterized by known frequencies but unknown amplitude, phase, and bias term. The presented scheme removes the essential strictly positive real (SPR)-like condition of the system, relaxing the prerequisite knowledge regarding the frequency response. The stability of the closed-loop system is illustrated using the small-gain theorem and Lyapunov-based analysis. Essentially, the developed regulator achieves complete cancellation of the external disturbance and drives the system output to zero, even in the presence of large system structural and parametric uncertainty. Through numerical simulation and hardware experiments on an active noise control (ANC) platform, we have substantiated the effectiveness of the proposed methodology.**

***Index Terms*— Disturbance rejection, active noise control, discontinuous control, uncertain systems, adaptive control**

I. Introduction

IN the field of control theory and its applications, the capacity of a dynamic system to reject the external disturbances plays a vital role in attaining the desired performance. Within the realm of disturbance rejection, the cancellation of periodic signals holds remarkable significance due to myriad applications in industry such as vibration suppression [1], spacecraft attitude control [2], active rotor balancing [3], and notably, in the field of active noise cancellation [4], [5].

Numerous established methodologies have been developed to effectively tackle the challenge of disturbance rejection. A prevalent one is the application of the Internal Model Principle (IMP), which encompasses the integration of the disturbance dynamics within the compensatory framework [6], [7]. In the domain of continuous-time systems, the research utilizing IMP-based methodologies has been systematically explored. This body of work spans an extensive range of conditions, from systems with clearly-defined models and disturbances to scenarios where both elements are characterized by uncertainty, as documented in references [8]–[11]. Although a number of works are available for continuous-time systems, only a few are available for the discrete-time counterpart, which is needed for digital implementation. As a result, the majority of digital control applications [12], [13] are often simply discretized to yield discrete-time controllers. However, the application of these directly-discretized controllers in regulating discrete-time systems frequently falls short of achieving the desired performance, as exemplified in the cases presented in [14]. The relative underrepresentation of IMP-based methodologies in the discrete-time disturbance rejection area makes the study of output regulation for discrete-time systems of great interest.

When precise models of the system and external disturbances are available, convention IMP-based methods has been well extended to the discrete-time system [15], [16]. Yet, in numerous real-world scenarios [17], [18], either the system model or the disturbance information is highly uncertain, or even both. Hence, similar to the continuous-time field, the exploration of the minimal assumptions required to solve the discrete-time harmonic disturbance rejection problem has been an attractive topic since then. One time-honored Higher Harmonic Control (HHC) [19], [20] is able to handle the scenarios where both the system and disturbances are enveloped in uncertainty. However, HHC is contingent upon the system's ability to rapidly achieve a Harmonic Steady State (HSS) response, disregarding transient behaviors, which may not always be feasible [21]. Take the interactive dynamic between the controller and plant into account, previous studies [22], [23] have introduced adaptive regulators to address scenarios where the plant model and the order of the disturbance model are known. Later in [24]–[26] the constraints of precise plant model was relaxed to accommodate some parameters uncertainty, under the premise of an identifiable structure. However, these approaches instead require the frequency information of disturbances. Solution in [27] can handle the completely unknown disturbances case and unknown plant model, but the plant has to be minimum phase with a known relative degree. Moreover, the convergence property in [27] is not exponential. The lasted results in the IMP-based disturbance compensator is introduced in [14], which achieve exponential cancellation. It requires only the plant to be internal stable and the sign of either the real or imaginary part of the system's transfer function at each disturbance frequency(the so-called SPR-like condition) is known. Recent AFC described in [10] and [11], has removed the internally stable requirement and SPR-like condition, respectively. However, these two innovations are exclusive to continuous-time systems, once again highlighting the lag in controller development for discrete-time systems.

It is worth mentioning that, with the development of sensor

This work was supported in part by the Yangfan Program of Shanghai, China, under Grant 21YF1429600. Corresponding author: Yang Wang.

Jiangkun Xu, Yizhou Gong (co-first author) and Yang Wang are with the School of Information Science and Technology, ShanghaiTech University, Shanghai 201210, China (e-mail:{xujk, gongyzh2022, wangyang4}@shanghaitech.edu.cn).

technology and computation efficiency, data-driven control provides effective alternative solutions by employing learning technique for model-absence scenarios [28]–[30]. Learning-based methods [31]–[33] have been employed in the domain of control to address disturbance rejection in discrete-time systems. However, its practical application is circumscribed by several pivotal factors. These include a reliance on extensive offline training data, sensitivity to the quality and quantity of data, high computational requirements, and a lack of robust theoretical guarantees [34].

Drawing upon the preceding discussions, we contend that adaptive control methodologies, with their aptitude for online computation and instantaneous adaptability, offer tangible advantages in contexts that tackle the challenges of disturbance rejection in discrete-time systems. Expanding upon our foundational research in continuous-time adaptive methodologies as documented in [11], this study ventures into the discrete-time domain. It has been noted that directly discretizing a continuous-time control strategy may inadvertently induce instability, given certain sampling intervals and frequencies—a caveat we expound upon in our Preliminaries. Consequently, this paper is dedicated to the tailored design of discrete-time controllers, aimed at meeting precise performance standards. However, we identify two primary challenges: the pervasive uncertainty in system structure and parameters, and the limited knowledge of external disturbances, with the amplitude, phase, and offset remaining indeterminate.

In this work, we seek minimal conditions for addressing disturbance rejection within uncertain discrete-time linear systems. This notably eliminates the necessity for conditions like the SPR-like condition, the sign of high-frequency gain, and the dimension and relative degree of the plant. In addition, no offline data for identification or training is needed. These advantages make the approach more applicable across a diverse array of applications. The proposed controller can be regarded as a pure data-driven technique, relying solely on output information, offering a distinct advantage over traditional physical modeling. This enables effective neutralization of external disturbances, even without any structural prior knowledge of the system model. It is particularly well-suited to scenarios where modeling proves infeasible that renders model-based strategies impractical. We innovatively implemented the proposed method in an ANC platform, where the conventional system identification techniques are not necessary here. Moreover, in the presence of multi-harmonic disturbances, the proposed controller operates on each frequency term separately without performance deterioration. Finally, simulations indicate that the system exhibits over-parameterization capability as the frequency components of the disturbance decrease.

Notation: $\mathbb{R}$ and $\mathbb{N}$ denote the set of real numbers and the set of natural numbers, respectively. $\|\cdot\|$ is the Euclidean norm and $\|\cdot\|_{\mathcal{L}_2}$ denotes the $\mathcal{L}_2$ norm for signals. $\mathcal{N}$ is the set $\{1, ..., N\}$. I denotes the identity matrix with the appropriate dimension. $\mathrm{blkdiag}(\cdot)$ denotes the block diagonal matrix. The linear oprator $\mathbf{I}(\cdot) : \mathbb{R}^{N+1} \to \mathbb{R}^{(2N+1)\times(2N+1)}$ is defined as $\mathbf{I}(u) := \oplus_{n=0}^{N} u_n I$, where $\oplus$ denotes the direct sum. $\Delta x(k)$ denotes feedforward difference, i.e., $\Delta x(k) = x(k+1) - x(k)$.

II. Problem Formulation and Preliminaries

A. Motivation

As outlined in the introduction, direct discretization can lead to several potential issues, such as sampling rate mismatch, computational complexity, and implementation limitations, or even results in instability. Next, we present a specific example that illustrates this problem.

Consider a linear, stable, and non-minimum phase continuous-time system described by $W(s) = \frac{2(s-1)}{s^2+2s+5}$. The plant is subjected to an external disturbance $d(t) = 2\sin(\omega_c t)$, where ω_c represents the disturbance frequency. We apply the novel AFC method proposed in our previous work [11] to mitigate the influence of disturbances. This controller has been rigorously proved to effectively eliminate the impact caused by the sinusoidal disturbance, as illustrated in Fig. 1.

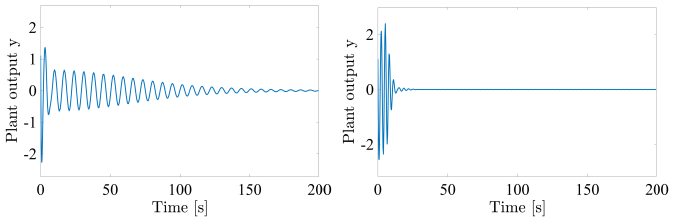

(a) (b)

Fig. 1. The proposed continuous-time AFC effectively achieves disturbance rejection in system $\boldsymbol{W(s)}$. (a) The case of disturbance frequency $\boldsymbol{\omega_c = 1}$ rad/s; (b) The case of disturbance frequency $\boldsymbol{\omega_c = 2}$ rad/s.

Upon implementing Euler's first-order discretization to the continuous-time controller [11], a discrete-time version can be easily derived. To assess the efficacy of this discretization approach on the discrete-time system, extensive numerical simulations were conducted across a spectrum of sampling times and disturbance frequencies. For instance, consider a sampling time of $T = 0.1\,\mathrm{s}$, which transforms the continuous-time system $W(s)$ into its discrete-time equivalent $H(z) = \frac{z-1.1}{z^2-1.4z+0.53}$, while the continuous-time disturbance $d(t)$ into $d(k) = 2\sin(\omega_d k)$. Note that $\omega_d = \omega_c T$ denotes the discrete-time frequencies. The results, as depicted in Fig. 2, clearly demonstrate that the directly discretized controller fails to regulate the output and cause the instability to the discrete-time system.

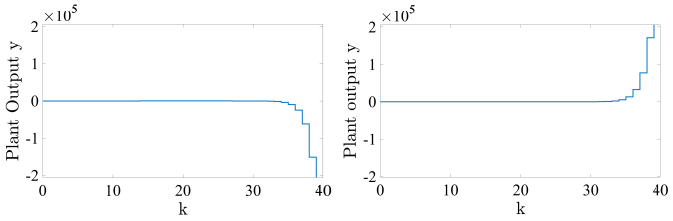

(a) (b)

Fig. 2. The instability of direct discretization approach occurs for certain sampling time $\boldsymbol{T}$ and certain frequency $\boldsymbol{\omega_c}$. (a) Setting the sampling time $\boldsymbol{T = 0.1\,\mathrm{s}}$ and disturbance frequency $\boldsymbol{\omega_c = 1\,\mathrm{rad/s}}$; (b) Setting the sampling time $\boldsymbol{T = 0.1\,\mathrm{s}}$ and disturbance frequency $\boldsymbol{\omega_c = 2\,\mathrm{rad/s}}$.

B. Problem formulation

We aim to study the disturbance rejection problem of discrete-time dynamical system modeled by

$$\begin{aligned} x(k+1) &= Ax(k) + B\big[u(k) - d(k)\big] \\ y(k) &= Cx(k) \end{aligned} \tag{1}$$

where $k \in \mathbb{N}$, $x(k) \in \mathbb{R}^n$, $u(k) \in \mathbb{R}$ and $y(k) \in \mathbb{R}$ denote the time index, system state, input and output, respectively. $A \in \mathbb{R}^{n\times n}$, $B \in \mathbb{R}^n$ and $C^\top \in \mathbb{R}^n$, involved in the system dynamics (1), are *unknown* constant matrices. Moreover, the transfer function for system (1) is defined as $H(z) := C\big(zI - A\big)^{-1}B$. $d(k) \in \mathbb{R}$ is a biased multi-sinusoidal disturbance, taking on the following form:

$$d(k) = \psi_0 + \sum_{i=1}^{N}\big[\psi_{i,1}\cos(\omega_i k) + \psi_{i,2}\sin(\omega_i k)\big] \tag{2}$$

with *unknown* bias $\psi_0 \in \mathbb{R}$, *unknown* parameters $\psi_{i,1}, \psi_{i,2} \in \mathbb{R}$, $i \in \mathcal{N}$ containing information of amplitudes and phases, and N distinct *known* frequencies $\omega_i \in \mathbb{R}_{>0}$, $i \in \mathcal{N}$. Given that the sampling time T of modern computers is typically quite small, the discrete-time frequencies are correspondingly low. For the convenience of subsequent mathematical derivations, we assume that $\omega_i \in (0, \frac{\pi}{2})$ for all $i \in \mathcal{N}$, without loss of generality. Our target is to identify the minimal assumptions necessary such that the disturbance (2) applied to system (1) can be completely suppressed. To focus on this issue, we proceed with the assumption that plant model (1) exhibits internal stability, as delineated below:

Assumption 1: A is a Schur matrix, there exist constants $\bar{c}_a > \underline{c}_a > 0$ such that the unique positive-definite solution $P_a \in \mathbb{R}^{n\times n}$ of the discrete Lyapunov equation

$$A^\top P_a A - P_a = -I$$

satisfies $\underline{c}_a I \le P_a \le \bar{c}_a I$.

Assumption 1 requires the system to be internal stable. Such an assumption is not conservative and quite standard in the area of the IMP-based output regulation [12], [14] especially for those focusing on disturbance rejection. Note that the rationale behind adopting this assumption is to elucidate the core focus more effectively. Consequently, systems that do not inherently exhibit internal stability lie outside the main ambit of this paper. This stems from the fact that a wide array of existing stabilized controllers are well-equipped to readily ensure internal stability. By simply adding these controllers with our proposed disturbance compensator, the objective of effective disturbance rejection can be achieved without necessitating the redesign of controllers. The problem that this paper aims to address is formally stated as follows:

Problem 1: Let Assumption 1 hold for the uncertain discrete-time plant (1) affected by the multi-sinusoidal disturbance (2). Design a dynamic feedback controller

$$\begin{aligned} \zeta(k+1) =& f(\zeta(k), y(k)), \zeta(0) = \zeta_0 \in \mathbb{R}^m \\ u(k) =& h(\zeta(k), y(k)) \end{aligned} \tag{3}$$

such that the trajectory of the closed-loop system originating from arbitrary initial conditions $x_0 \in \mathbb{R}^n$, $\zeta_0 \in \mathbb{R}^m$ are bounded and the output of plant satisfies $\lim_{k\to\infty} y(k) = 0$.

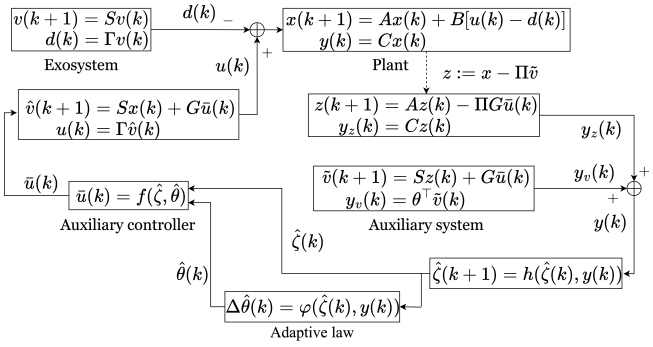

Fig. 3. Schematic illustration of the controller design.

III. Controller Design

A. Certainty equivalence controller design

A concise schematic diagram of the controller's design is presented in Fig. 3. We begin by modeling the multi-sinusoidal disturbance (2) to be the output of following discrete-time exosystem

$$\begin{aligned} v(k+1) &= Sv(k) \\ d(k) &= \Gamma v(k) \end{aligned} \tag{4}$$

where $v(k) \in \mathbb{R}^{2N+1}$ is the state, $S := \mathrm{diag}(1, s_1, \ldots, s_N) \in \mathbb{R}^{(2N+1)\times(2N+1)}$, $\Gamma^\top := [1, g^\top, \ldots, g^\top]^\top \in \mathbb{R}^{2N+1}$, with

$$s_i := \begin{bmatrix} \cos\omega_i & \sin\omega_i \\ -\sin\omega_i & \cos\omega_i \end{bmatrix},\ g := [1, 0]^\top,\ i \in \mathcal{N}. \tag{5}$$

Now, we articulate the requisite frequency response as entailed by the previously mentioned SPR-like condition. Building on Assumption 1, given the condition that A and -S do not share any eigenvalues, there exists a unique matrix $\Pi \in \mathbb{R}^{n\times(2N+1)}$ that uniquely satisfies the Sylvester equation

$$\Pi S = A\Pi + B\Gamma.$$

It is crucial to emphasize that A and B are matrices with unknown values, the matrix Π consequently remains unidentified. Define the steady state $x_{ss}(k) := -\Pi v(k)$ and the steady state error $\tilde{x}_{ss}(k) := x(k) - x_{ss}(k)$. When $u \equiv 0$, we have

$$\begin{aligned} \tilde{x}_{ss}(k+1) &= x(k+1) - x_{ss}(k+1) \\ &= Ax(k) - B\Gamma v(k) + \Pi S v(k) \\ &= A\tilde{x}_{ss}(k) \end{aligned}$$

which indicates that x converges to x_{ss} exponentially fast and the steady state of the output $y_{ss}(k)$ admits the form

$$y_{ss}(k) = Cx_{ss}(k) = -C\Pi v(k). \tag{6}$$

On the other hand, considering the frequency response characteristics of discrete-time linear systems, the steady-state response adheres to the following form

$$y_{ss}(k) = -\vartheta^\top v(k) \tag{7}$$

where the unknown vector ϑ corresponds to the system's frequency response at different frequencies, is denoted by

$$\vartheta^\top := \big[\vartheta_0, \vartheta_1^\top, \ldots, \vartheta_N^\top\big] \tag{8}$$

with $\vartheta_0 := H(e^0)$ and

$$\vartheta_i^\top = [\vartheta_{i,1}\ \vartheta_{i,2}] := \big[\mathrm{Re}\{H(e^{j\omega_i})\},\ \mathrm{Im}\{H(e^{j\omega_i})\}\big], \quad i \in \mathcal{N}.$$

Considering equation (6) and (7), the unknown frequency response parameter vector $\vartheta^\top = C\Pi$. This relation provides a crucial equivalence for the unknown parameters, deemed essential in prior research, embodying what is known as the SPR-like condition. To circumvent the necessity of the SPR-like condition, we adopt the ensuing weaker assumption.

Assumption 2: The unknown parameter vector (8) satisfies $\vartheta_0 \in \Theta_0 \subset \Theta$ (abbreviated as $\vartheta_0 \in \Theta$ for ease of notation) and $\vartheta_i \in \Theta$ for all $i \in \mathcal{N}$, where Θ_0 and Θ are given by

$$\Theta_0 := \{\vartheta \in \mathbb{R} \mid r_1^2 \le |\vartheta| \le r_2^2\}$$
$$\Theta := \{\vartheta \in \mathbb{R}^2 \mid r_1^2 \le \|\vartheta\|^2 \le r_2^2\}$$

for some known positive numbers $0 < r_1 < r_2$. Concurrently, the domain of ϑ is denoted as $\vartheta \in \Theta^{N+1}$, encapsulating the collective parameter space[1]. ◁

Assumption 2 presented here significantly relax the SPR-like condition required in [14] in the sense that it is independent of the sign of the elements of ϑ. Therefore, the sign of $H(e^0)$, $\mathrm{Re}\{H(e^{j\omega_i})\}$ and $\mathrm{Im}\{H(e^{j\omega_i})\}$, $i \in \mathcal{N}$, can change over the frequencies of interest, which is not permitted in some SPR-like condition for instance the minimum-phase assumption in [10]. Moreover, Assumption 2 is practical feasible in the sense that in practical scenarios, one can always select sufficiently small r_1 and sufficiently large r_2 to satisfy this assumption. While these bounds can be distinct, especially when partial prior knowledge is accessible, we opt for uniformity in their selection here to simplify the mathematical exposition.

To cancel the disturbances $d(k)$ in a feedforward manner, we consider the controller:

$$\begin{aligned} \hat{v}(k+1) &= S\hat{v}(k) + G\bar{u}(k) \\ u(k) &= \Gamma\hat{v}(k) \end{aligned} \tag{9}$$

where $G := \mathrm{diag}(1, g, ..., g) \in \mathbb{R}^{(2N+1)\times(N+1)}$, $\hat{v}(k) \in \mathbb{R}^{2N+1}$, and $\bar{u}(k) = \mathrm{col}(\bar{u}_0, \ldots, \bar{u}_N) \in \mathbb{R}^{N+1}$ is an auxiliary input to be defined. To facilitate the design of the auxiliary input, we employ the coordinate transformation $\tilde{v} := \hat{v} - v \in \mathbb{R}^{2N+1}$ and $z := x - \Pi\tilde{v} \in \mathbb{R}^n$. This yields the subsequent error system

$$\begin{aligned} z(k+1) &= Az(k) - \Pi G\bar{u}(k) \\ \tilde{v}(k+1) &= S\tilde{v}(k) + G\bar{u}(k) \\ y(k) &= Cz(k) + \vartheta^\top\tilde{v}(k). \end{aligned} \tag{10}$$

The estimation error $\tilde{v}$ within (10) is analyzed independently and reformulated as follows

$$\begin{aligned} \tilde{v}(k+1) &= S\tilde{v}(k) + G\bar{u}(k) \\ y_v(k) &= \vartheta^\top\tilde{v}(k)\,. \end{aligned} \tag{11}$$

Under Assumption 2, the dynamics presented in equation (11) satisfy controllability and observability. Given that ϑ is unknown, the current form of equation (11) does not permit the design of an observer. It necessitates the application of a coordinate transformation $\zeta(k) := D^{-1}\tilde{v}(k) \in \mathbb{R}^{2N+1}$, where $D := \mathrm{diag}(\vartheta_0^{-1}, D_1, \ldots, D_N) \in \mathbb{R}^{(2N+1)\times(2N+1)}$, with

$$D_i := \frac{1}{\vartheta_{i,1}^2 + \vartheta_{i,2}^2}\begin{bmatrix} \vartheta_{i,1} & -\vartheta_{i,2} \\ \vartheta_{i,2} & \vartheta_{i,1} \end{bmatrix}, \quad i \in \mathcal{N}\,. \tag{12}$$

Following this transformation, we obtain a new representation of the exosystem's estimation error dynamics

$$\begin{aligned} \zeta(k+1) &= S\zeta(k) + \theta\bar{u}(k) \\ y_v(k) &= \Gamma\zeta(k) \end{aligned} \tag{13}$$

where $\theta := \mathrm{diag}(\theta_0, \theta_1, \ldots, \theta_N) \in \mathbb{R}^{(2N+1)\times(N+1)}$ is a block diagonal matrix that contains the unknown parameters, with $\theta_0 := \vartheta_0 \in \Theta$ and $\theta_i := [\vartheta_{i,1}\ \ -\vartheta_{i,2}]^\top \in \Theta$ for all $i \in \mathcal{N}$, owing to the Assumption 2. If θ and ζ are available, then designing $\bar{u} = \bar{u}^* := -\varepsilon\theta^\top\zeta$ to ensure system (13) converges to zero exponentially fast becomes straightforward, allowing system (9) to effectively track the exosystem and regenerate the disturbances. Consequently, in scenarios where θ and ζ are not available, an adaptive observer for system (13) is outlined as follows

$$\begin{aligned} \hat{\zeta}(k+1) &= S\hat{\zeta}(k) + \hat{\theta}(k)\bar{u}(k) - \varepsilon\Gamma^\top\big[\hat{y}_1(k) - y(k)\big] \\ \hat{y}_v(k) &= \Gamma\hat{\zeta}(k) \end{aligned}$$

where $\hat{\theta}(k) := \mathrm{diag}(\hat{\theta}_0(k), \hat{\theta}_1(k), \ldots, \hat{\theta}_N(k))$ is the estimate of θ and $\varepsilon > 0$ is a gain parameter. Then we present the form of the certainty-equivalence control law

$$\bar{u}(k) = -\varepsilon\hat{\theta}^\top(k)\hat{\zeta}(k). \tag{14}$$

Thus, the observer dynamics is transformed into

$$\Sigma_0 : \begin{cases} \hat{\zeta}(k+1) = E(k)\hat{\zeta}(k) - \varepsilon\Gamma^\top\big[\hat{y}_v(k) - y(k)\big] \\ e_0(k) = \hat{\theta}^\top(k)\hat{\zeta}(k) \end{cases} \tag{15}$$

where $E(k) := S - \varepsilon\hat{\theta}(k)\hat{\theta}^\top(k) \in \mathbb{R}^{(2N+1)\times(2N+1)}$. The dynamics of observation error $\tilde{\zeta}(k) := \hat{\zeta}(k) - \zeta(k) \in \mathbb{R}^{2N+1}$ is given by the following equation

$$\begin{aligned} \tilde{\zeta}(k+1) &= F\tilde{\zeta}(k) + \tilde{\theta}(k)\bar{u}(k) + \varepsilon\Gamma^\top Cz(k) \\ \tilde{y}(k) &= \Gamma\tilde{\zeta}(k) - Cz(k) \end{aligned} \tag{16}$$

where $F := S - \varepsilon\Gamma^\top\Gamma \in \mathbb{R}^{(2N+1)\times(2N+1)}$, $\tilde{\theta}(k) := \hat{\theta}(k) - \theta \in \mathbb{R}^{2N+1}$, $\tilde{y}(k) := \hat{y}_v(k) - y(k) \in \mathbb{R}$. By employing the discrete Lyapunov theory, we derive the following properties for two critical matrices, E and F, within the systems (15) and (16), respectively, for the following analysis:

Property 1: Let $\mathbf{I}_e(\theta, \varepsilon)$ be the positive-definite diagonal matrix-valued function

$$\mathbf{I}_e(\theta, \varepsilon) := \varepsilon\,\mathrm{blkdiag}(\theta_0, \theta_1^\top\theta_1 \cdot I_2, \ldots, \theta_N^\top\theta_N \cdot I_2)$$

and let $P_e(\theta, \varepsilon) \in \mathbb{R}^{(2N+1)\times(2N+1)}$ denote the solution of the following discrete Lyapunov equation

$$E^\top(\theta)P_e(\theta, \varepsilon)E(\theta) - P_e(\theta, \varepsilon) = -\mathbf{I}_e(\theta, \varepsilon) \tag{17}$$

where $E(\theta) := S - \varepsilon\theta\theta^\top$. There exists a scalar $\bar{\varepsilon}_e > 0$ and constants $\bar{c}_e > \underline{c}_e > 0$, $\bar{e} > 0$ such that $\|E(\theta)\| \le \bar{e}I$ and $\underline{c}_e I \le P_e \le \bar{c}_e I$ for all $(\theta, \varepsilon) \in \Theta^{N+1} \times (0, \bar{\varepsilon}_e)$.

[1]Each frequency component ϑ_i lies within Θ, and with a total of $N+1$ frequency components, the entire set of ϑ is expressed as belonging to Θ^{N+1}.

Property 2: Let $P_f(\varepsilon)$ denote the symmetric solution of the family of discrete Lyapunov equations

$$F^\top P_f(\varepsilon)F - P_f(\varepsilon) = Q_f(\varepsilon) \tag{18}$$

for some symmetric negative-definite matrix-valued function $Q_f(\varepsilon)$. There exist scalars $\bar{\varepsilon}_f > 0$, $\alpha > 0$, $\bar{c}_f > \underline{c}_f > 0$ and $\bar{f} > 0$ such that $\|F\| \leq \bar{f}I$, $Q_f \leq -\varepsilon\alpha I$ and $\underline{c}_f I \leq P_f \leq \bar{c}_f I$ for all $\varepsilon \in (0, \bar{\varepsilon}_f)$.

Due to space constraints, the proofs of these two properties are not included here; please refer to the supplementary materials for details.

B. Non-minimal realization of the observation error dynamics

To formulate an adaptive law for parameter estimation $\hat{\theta}(k)$, it is crucial to clearly define the linear relationship between key parameters and an observable state. This task is critical in establishing a formal foundation for the design of the parameter update law in the next Section. Consequently, it is imperative to construct a model that ensures a certain degree of observability through the establishment of a non-minimal realization state-space model, achieved via appropriate coordinate transformation.

The observation error system (16) can be decomposed into the following components

$$\tilde{y}_a(k) = \Gamma \sum_{j=0}^{k-1} F^{k-j-1}\tilde{\theta}(j)\bar{u}(j) \tag{19}$$

$$\tilde{y}_b(k) = \varepsilon\Gamma \sum_{j=0}^{k-1} F^{k-j-1}\Gamma^\top C z(j) - Cz(k). \tag{20}$$

with $\tilde{y} = \tilde{y}_a + \tilde{y}_b$. Our analysis begins by focusing on the subsystem (19). Defining

$$\Psi(j) = \sum_{i=0}^{j-1} F^{-i}\mathbf{I}(\bar{u}(i)) \in \mathbb{R}^{(2N+1)\times(2N+1)},$$

we derive the forward difference equation $\Delta\Psi(j) = F^{-j}\mathbf{I}(\bar{u}(j))$, which yields

$$\tilde{y}_a(k) = \Gamma F^{k-1} \sum_{j=0}^{k-1} \Delta\Psi(j)\tilde{\theta}(j).$$

Applying the Abel transformation [35], we can refine the formulation of the $\tilde{y}_a$ as $\tilde{y}_a = e_1 - e_2$, detailed as follows

$$\begin{aligned}\tilde{y}_a(k) =& \underbrace{\Gamma F^{k-1} \sum_{j=0}^{k-1} \Delta\Psi(j)\tilde{\theta}(k)}_{e_1} \\ & \underbrace{- \Gamma F^{k-1} \sum_{j=1}^{k-1} \Psi(j+1)\,\Delta\tilde{\theta}(j)}_{e_2}.\end{aligned} \tag{21}$$

The first term e_1 in (21) can be represented in the following state-space equation

$$\Sigma_1 : \begin{cases} \hat{\xi}_1(k+1) = F^\top\hat{\xi}_1(k) + G\bar{u}(k),\ \hat{\xi}_1(0) = \hat{\xi}_{1_0} \\ e_1(k) = \tilde{\theta}^\top(k)\hat{\xi}_1(k) \end{cases} \tag{22}$$

where we choose an observer signal $\hat{\xi}_1$ to substitute the state ξ_1, without loss of generality. Note that $\Psi(1) = 0$, the second term e_2 in (21) gives

$$\tilde{y}_{a,2}(k) = \Gamma \sum_{j=0}^{k-1} F^{k-j-1}\xi_a(j+1)\,\Delta\tilde{\theta}(j)$$

where $\xi_a(j+1) = \sum_{i=0}^{j} F^{j-i}\mathbf{I}(\bar{u}(i)) \in \mathbb{R}^{(2N+1)\times(2N+1)}$ admits the dynamics

$$\xi_a(k+1) = F\xi_a(k) + \mathbf{I}(\bar{u}(k)).$$

Consequently, e_2 is governed by the state-space equation

$$\Sigma_2 : \begin{cases} \xi_2(k+1) = F\xi_2(k) + \xi_a(k+1)\Delta\hat{\theta}(k) \\ \xi_a(k+1) = F\xi_a(k) + \mathbf{I}(u(k)) \\ e_2(k) = \Gamma\xi_2(k) \end{cases} \tag{23}$$

where $\xi_2(0) = \xi_{2_0} \in \mathbb{R}^{2N+1}$, and the estimation signal $\Delta\hat{\theta}(k)$ is a time-varying parameter vector to be specified. Thus far, we have fully described subsystem $\tilde{y}_a$ in (19). Next, we formulate the discrete-time linear dynamics for another subsystem, $\tilde{y}_b$, represented by e_3, as follows

$$\Sigma_3 : \begin{cases} \xi_3(k+1) = F\xi_3(k) + \varepsilon\Gamma^\top C z(k) \\ z(k+1) = Az(k) - \Pi G\bar{u}(k) \\ e_3(k) = \Gamma\xi_3(k) - Cz(k). \end{cases} \tag{24}$$

Through there formulations, we have successfully achieved the desired formulation, where the critical parameters and the observable state exhibit a clear linear relationship within the output expression, as illustrated by the following equation

$$y(k) = \Gamma\zeta(k) - \tilde{\theta}^\top(k)\hat{\xi}_1(k) + \Gamma\xi_2(k) - \Gamma\xi_3(k) + Cz(k) \tag{25}$$

where equations (15), (22), (23), and (24) are considered.

IV. Adaptive Law Design

The findings delineated in Section III have focused on modeling disturbances and devising a feedforward compensator (9), alongside proposing an auxiliary control law (14). Subsequently, the error system is framed as a non-minimal realization (25), laying the groundwork for our forthcoming parameter update law design. This adaptive law will provide estimates of frequency response of the system, $\hat{\theta}(k)$, which facilitates the elimination of the SPR-like condition and serves as a crucial component of the auxiliary controller (14).

Concurrently, it is imperative to note that the parameter set Θ, assumed under Assumption 2, is non-convex. Bounding the estimates away from the origin is essential to guarantee the observability of the system. To address this, we partition the non-convex feasible domain of the estimations into several bounded convex subsets and introduce a multi-model adaptive control paradigm. As illustrated in Fig. 4, θ_i, $i \in \mathcal{N}$ (θ_0 is treated in the similar manner) denotes the system's frequency response information for a specific frequency, and $\hat{\theta}_i(k)$ represents its estimate. Both θ_i and $\hat{\theta}_i(k)$ can occupy any position within the non-convex set Θ.

We then propose a multi-domain set approach, supplanting the original single non-convex set Θ and incorporating multi-model adaptive control to address the issue of switching

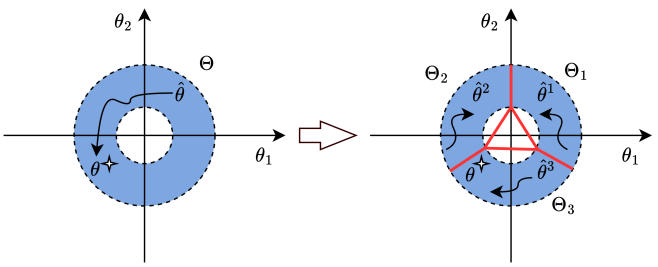

Fig. 4. Finite covering of $\boldsymbol{\Theta}$ using three convex sets $\boldsymbol{\Theta_n}$, $\boldsymbol{n = 1, 2, 3}$.

estimates across multiple domains. Any estimate within this subspace Θ_j, $j \in \mathcal{Q} := \{1, 2, 3\}$, is guaranteed not to induce unobservability within the system's state.

With the introduction of the multi-model switching mechanism, each parameter estimates $\hat{\theta}_i^j$, $i \in \mathcal{N}$, $j \in \mathcal{Q}$ (for $i = 0$, $j \in \{1, 2\}$) is required to evolve within a specific convex set Θ_j. Within this framework, we update the dynamics of the observer signal $\hat{\zeta}$ in (15) and the adaptive controller $\bar{u}$ in (14) to the following form for each excitation frequency

$$\begin{aligned} \hat{\zeta}_i^j(k+1) &= S\hat{\zeta}_i^j(k) + \hat{\theta}_i^j(k)\bar{u}_i^{\sigma_i}(k) - \varepsilon g\tilde{y}_i^j(k) \\ \tilde{y}_i^j(k) &= g^\top \hat{\zeta}_i^j(k) - y_i(k) \\ \bar{u}_i^{\sigma_i}(k) &= -\varepsilon \hat{\theta}_i^{\sigma_i\top}(k)\hat{\zeta}_i^{\sigma_i}(k) \end{aligned} \tag{26}$$

For any step $k \geq 0$, the control signal $\bar{u}_i(k)$ is selected as $\bar{u}_i^{\sigma_i(k)}(k)$, where $\sigma := (\sigma_0 \cdots \sigma_N)$ and $\sigma_i : \mathbb{N}_{\geq 0} \mapsto \mathcal{Q}$ is a piecewise-constant switching signal taking value in $\{1, 2, 3\}$, guided by the switching mechanism to be designed. Leveraging the observable signal $\hat{\xi}_1$ and $\tilde{y}$, we formulate an update law as follows

$$\begin{aligned} \Delta\hat{\theta}_i^j(k) &= \mathrm{Proj}\Big(\hat{\theta}_i^j(k), \varphi_i^j\big(\hat{\xi}_{1i}(k), \tilde{y}_i^j(k)\big)\Big) \\ y_i(k) &= y(k) - \sum_{m=0, m\neq i}^{N} g^\top \hat{\zeta}_m^{\sigma_m}(k), \ j \in \mathcal{Q}, \ i \in \{0\} \cup \mathcal{N} \end{aligned} \tag{27}$$

where the parameter estimates are given by $\hat{\theta}^\sigma = \mathrm{col}(\hat{\theta}_0^{\sigma_0\top}, \cdots, \hat{\theta}_N^{\sigma_N\top})$ with the initial value of $\hat{\theta}_i^j(k)$ situated within $\mathrm{int}\Theta_j$. A normalized gradient law is employed as the unconstrained update law $\varphi^j : (\hat{\xi}_1, \tilde{y}^j) \mapsto \mathbb{R}^{2N+1}$ for each estimator, where

$$\varphi_i^j(\hat{\xi}_{1i}, \tilde{y}_i^j) = -\frac{\rho\varepsilon^2}{N+1}\frac{\hat{\xi}_{1i}\tilde{y}_i^j}{m_i^{j2}}, \quad \forall j \in \mathcal{Q}, i \in \{0\} \cup \mathcal{N} \tag{28}$$

results in $\varphi^j(\hat{\xi}_1, \tilde{y}^j) = \mathrm{col}\big(\varphi_0^j(\hat{\xi}_{10}, \tilde{y}_0^j), \ldots, \varphi_N^j(\hat{\xi}_{1N}, \tilde{y}_N^j)\big)$. The normalizing term m_i^{j2} is defined as $m_i^{j2} := 1 + \|\hat{\xi}_{1i}\|^2 + |\tilde{y}_i^j|^2$, ensuring the condition $\|\varphi^j\| < \rho\varepsilon^2$ for all $j \in \mathcal{Q}$ is met. $\mathrm{Proj}(\cdot)$ is the standard gradient projection, ensuring that the frequency response estimate generated by each estimator remains confined to its corresponding subspace. For clarity, we illustrate the projection of the unconstrained estimates onto Θ_1 (corresponding to Fig. 4) as an example, given by:

$$\mathrm{Proj}\left(\hat{\theta}_i^1, \varphi^1\right) = \varphi^1 - \mathcal{I}\left(\hat{\theta}_i^1, \varphi^1\right)\varphi^1,$$

where

$$\mathcal{I}\left(\hat{\theta}_i^1, \varphi\right) = \begin{cases} \frac{\hat{\theta}_i^1\hat{\theta}_i^{1\top}}{\|\hat{\theta}_i^1\|^2} & \text{if } \|\hat{\theta}_i\| = r_2 \text{ and } \varphi^\top\hat{\theta}_i > 0 \\ \mathbf{e}\mathbf{e}^\top & \text{if } \sqrt{3}\hat{\theta}_{i,1}^1 + \hat{\theta}_{i,2}^1 = r_1 \text{ and } \varphi^\top\mathbf{e} < 0 \\ \mathbf{e_x}\mathbf{e_x}^\top & \text{if } \frac{1}{\sqrt{3}}\hat{\theta}_{i,1}^1 + \hat{\theta}_{i,2}^1 = 0 \text{ and } \varphi^\top\mathbf{e_x} < 0 \\ \mathbf{e_y}\mathbf{e_y}^\top & \text{if } \hat{\theta}_{i,2}^1 = 0 \text{ and } \varphi^\top\mathbf{e_y} < 0 \\ 0 & \text{otherwise} \end{cases}$$

and $\mathbf{e} := \left(\frac{\sqrt{3}}{2}, \frac{1}{2}\right)^\top$, $\mathbf{e_x} := \left(\frac{1}{2}, \frac{\sqrt{3}}{2}\right)^\top$, $\mathbf{e_y} := (1, 0)^\top$.

In light of the multi-model control strategies, we introduce the creation of corresponding performance indices J_i^j for each estimator subset at each excitation frequency to facilitate the selection of the optimal controller. The designed index J_i^j will reflect the difference between the estimated and true values, thereby guiding the design of an appropriate controller switching logic. The performance criteria guiding the switching logic are encapsulated by the functions defined as follows

$$J_i^j(k) = \beta\sum_{\tau=0}^{k-1}\tilde{y}_i^j(\tau)^2, \quad j \in \mathcal{Q}, \ i \in \{0\} \cup \mathcal{N} \tag{29}$$

where $\beta > 0$ is a parameter to be selected.

Moreover, to prevent excessively frequent switching, we introduce a hysteresis switching mechanism. Let the time sequence $\{T_m\}_{m=1}^M$ denote the instances at which switching occurs, with $M \leq \infty$. First, we set $\sigma_i(0) = \arg\min_{j\in\mathcal{Q}}\{J_i^j(0)\}$. By determining a hysteresis constant $h \in \mathbb{R}> 0$, the hysteresis mechanism's switching logic is formally stated as

$$\sigma_i(T_m) := \arg\min_{j\in\mathcal{Q}}\left\{J_{ih}^j(T_m)\right\}, \ \forall i \in \{0\} \cup \mathcal{N} \tag{30}$$

where

$$J_{ih}^j(T_m) := \begin{cases} J_i^j(T_m) & \text{if } j = \sigma_i(T_{m-1}) \\ J_i^j(T_m) + h & \text{if } j \neq \sigma_i(T_{m-1}) \end{cases}.$$

The multi-model controller here features relatively low dimensionality, comprising $3N$ estimators, each with four states. An illustrative schematic of this controller is shown in Fig. 5. Meanwhile, the switching adaptive algorithm ensures the following outcomes. Due to space constraints, the proof of the following Lemmas is omitted; please refer to the supplementary materials for details.

Property 3: For all $j \in \mathcal{Q}$, the forward solutions $\Delta\hat{\theta}^j(k)$ of (27) and (28), satisfies $\hat{\theta}^j(k) \in \Theta^{N+1}$ and $\|\Delta\hat{\theta}^j(k)\| \leq \rho\varepsilon^2$, for all $k \geq 0$ and all initial conditions $\hat{\theta}^j(0) \in \mathrm{int}\,\Theta_j$.

Lemma 1: For the hysteresis switching mechanism in (30), a constant $\bar{\varepsilon}_t$ and a constant $T_s > 0$ exist, such that $\sigma(k) = \sigma(T_s)$ for any $k \in [T_s, +\infty)$ and $\varepsilon \in (0, \bar{\varepsilon}_t)$, that is, switchings stop at most in time steps T_s.

Lemma 2: The normalization signal $m_i^j(\cdot)$ in the update law (27) belongs to $\mathcal{L}_\infty$ for all $i \in \{0\} \cup \mathcal{N}$ and $j \in \mathcal{Q}$.

Remark 1: A specific instant, $T_s > 0$, signifies the termination of controller switching activities. In other words, for all $k \geq T_s$, the functioning dynamics of the multiple-model controller seamlessly align with those of the baseline controller framework presented in Section III.

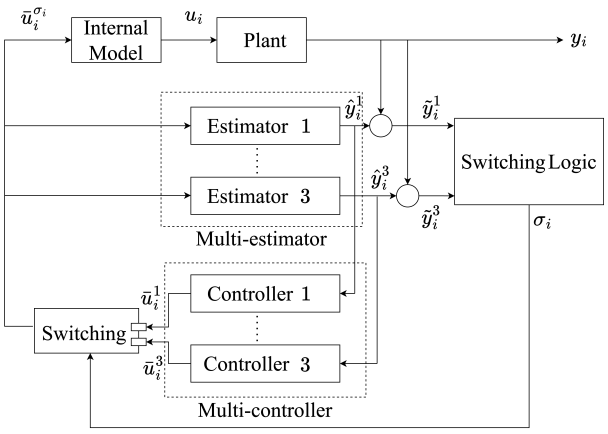

Fig. 5. Block diagram of the multi-model controller for each frequency $\boldsymbol{\theta_i}, \boldsymbol{i \in \{0\} \cup \mathcal{N}}$.

V. Stability Analysis

This section aims to establish the stability properties of the closed-loop system, particularly when employing the multi-model switching control strategy. Our core objective is to prove that all signals in the closed-loop system are bounded before switching stops, and that relevant signals converge after switching stops. Specifically, the implementation of the multiple-model switching controller leads to the formation of a new closed-loop system

$$\Sigma_0 : \begin{cases} \hat{\zeta}^{\sigma}(k+1) = E^{\sigma}(k)\hat{\zeta}^{\sigma}(k) + \varepsilon\Gamma^{\top}\nu_0(k) \\ e_0(k) = \hat{\theta}^{\sigma\top}(k)\hat{\zeta}^{\sigma}(k) \end{cases} \tag{31}$$

$$\Sigma_1 : \begin{cases} \hat{\xi}_1(k+1) = F^{\top}\hat{\xi}_1(k) - \varepsilon G\nu_1(k) \\ e_1(k) = \tilde{\theta}^{\sigma\top}(k)\hat{\xi}_1(k) \end{cases} \tag{32}$$

$$\Sigma_2 : \begin{cases} \xi_2(k+1) = F\xi_2(k) + \xi_a(k+1)\Delta\hat{\theta}^{\sigma}(k) \\ \xi_a(k+1) = F\xi_a(k) + \mathbf{I}(-\varepsilon\nu_2(k)) \\ e_2(k) = \Gamma\xi_2(k) \end{cases} \tag{33}$$

$$\Sigma_3 : \begin{cases} \xi_3(k+1) = F\xi_3(k) + \varepsilon\Gamma^{\top}Cz(k) \\ z(k+1) = Az(k) + \varepsilon\Pi G\nu_3(k) \\ e_3(k) = \Gamma\xi_3(k) - Cz(k) \end{cases} \tag{34}$$

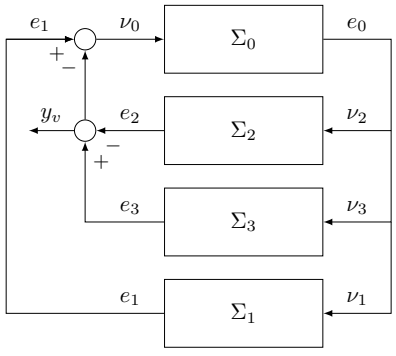

Fig. 6. Interconnection of subsystems $\boldsymbol{\Sigma_0}$-$\boldsymbol{\Sigma_3}$.

where $\nu_0 = e_1 + e_2 - e_3$, $\nu_1 = \nu_2 = \nu_3 = e_0$. This interconnection is depicted in Fig. 6. While the overall input is denoted as e_1, while the overall output is given by $y_v = e_3 - e_2$.

The subsequent propositions outline the stability features of the subsystems Σ_0, Σ_2 and Σ_3. This analysis utilizes dissipative system theory to conduct a detailed examination, employing finite-gain $\mathcal{L}_2$-$\mathcal{L}_\infty$ stability to rigorously assess their characteristics.

Proposition 1: There exist scalars $\gamma_0 > 0$ and $\bar{\varepsilon}_0 > 0$ such that subsystem Σ_0 is strictly dissipative with respect to the supply rate $q_0(\nu_0, e_0) = \gamma_0^2|\nu_0|^2 - \|e_0\|^2$ for all $\varepsilon \in (0, \bar{\varepsilon}_0)$, with quadratic, positive-definite and decrescent storage function $W_0(k) = 2\varepsilon^{-1}\hat{\zeta}^{\top}(k)P_e(k)\hat{\zeta}(k)$.

Proposition 2: There exists $\gamma_2 > 0$ and $\bar{\varepsilon}_2$ such that subsystem Σ_2 is strictly dissipative with respect to the supply rate $q_2(\nu_2, e_2) = \varepsilon^2\gamma_2^2\|\nu_2\|^2 - |e_2|^2$ for all $\varepsilon \in (0, \bar{\varepsilon}_2)$, with quadratic and positive-definite storage function $W_2(\xi_2, \xi_a)$.

Proposition 3: There exists $\gamma_3 > 0$ such that subsystem Σ_3 is strictly dissipative with respect to the supply rate $q_3(\nu_3, e_3) = \varepsilon^2\gamma_3^2\|\nu_3\|^2 - |e_3|^2$ for all $\varepsilon \in (0, \bar{\varepsilon}_3)$, with quadratic and positive-definite storage function $W_3(\xi_3, z)$.

The proofs of Propositions 1-3 can be easily derived by following the approach in [36]. Next, we present the main results of this paper as follows:

Theorem 1: Consider the discrete-time plant model (1) and the disturbance (2) under Assumptions 1-2. There exist positive constants $\bar{\varepsilon}$ and $\bar{\rho}$ such that the Problem 1 can be solved using the AFC-based method, consisting of (9), (14), (15) and (27), for any $\varepsilon \in (0, \bar{\varepsilon})$ and any $\rho \in (0, \bar{\rho})$.

Proof: Let $\varepsilon \in (0, \bar{\varepsilon}_0)$, according to Propositions 1-3, for any time interval $[0, \tau] = \bigcup_{m=1}^{\bar{m}}[T_{m-1}, T_m) \bigcup [T_{\bar{m}}, \tau]$, where $0 \leq T_{\bar{m}} \leq \tau < T_{\bar{m}+1}$, we have

$$\|e_{0_\tau}\|_{\mathcal{L}_2} \leq \gamma_0\|e_{1_\tau}\|_{\mathcal{L}_2} + \varepsilon\gamma_0(\gamma_2 + \gamma_3)\|e_{0_\tau}\|_{\mathcal{L}_2}$$

where $e_{1_\tau}(\cdot)$ is the truncation of the signal $e_1(\cdot)$ over time interval $[0, \tau]$. Defining $\bar{\varepsilon}_4 := \min\{\bar{\varepsilon}_e, \bar{\varepsilon}_f, \bar{\varepsilon}_0, \bar{\varepsilon}_2, \bar{\varepsilon}_3, \frac{1}{\gamma_0(\gamma_2+\gamma_3)}\}$, we can establish that subsystems Σ_0, Σ_2 and Σ_3 form a small-gain theorem interconnection (with respect to the $\mathcal{L}_2$-norm) for $\varepsilon \in (0, \bar{\varepsilon}_4)$. Application of the small-gain theorem gives

$$\begin{aligned} \|y_{v_\tau}\|_{\mathcal{L}_2}^2 &= \sum_{m=1}^{\bar{m}}\left[\sum_{s=T_{m-1}}^{T_m-1}|y_v(s)|^2 + \sum_{s=T_{\bar{m}}}^{\tau-1}|y_v(s)|^2\right] \\ &\leq \bar{c}_\varepsilon^2\|e_{1_\tau}\|_{\mathcal{L}_2}^2 \end{aligned}$$

where $\bar{c}_\varepsilon := \frac{\varepsilon\gamma_0(\gamma_2+\gamma_3)}{1-\varepsilon\gamma_0(\gamma_2+\gamma_3)}$, from which it can be concluded that

$$\|y_{v_\tau}\|_{\mathcal{L}_2} \leq \bar{c}_\varepsilon\|e_{1\tau}\|_{\mathcal{L}_2} \tag{35}$$

for all $\varepsilon \in (0, \bar{\varepsilon}_4)$ and all $\tau \in \mathbb{R}_{\geq 0}$.

Subsequently, we demonstrate that $e_1 \in \mathcal{L}_2$. Consider the storage function $V^{\kappa}(k) = \frac{1}{2}\|\tilde{\theta}^{\kappa}\|^2$, where $\tilde{\theta}^{\kappa} := \hat{\theta}^{\kappa} - \theta$ represents the estimation error with κ denoting the specific estimator. By analyzing the behavior of $V^{\kappa}(\tilde{\theta}^{\kappa})$ along the trajectories of the parameter estimates, as governed by the update law (27) and (28), reveals that

$$\Delta V^{\kappa}(k) = \mathrm{Proj}(\hat{\theta}^{\kappa}, \varphi^{\kappa}(\hat{\xi}_1, \tilde{y}^{\kappa})) \leq -\rho\varepsilon^2\tilde{\theta}^{\kappa\top}\frac{\hat{\xi}_1\tilde{y}^{\kappa}}{m_\kappa^2}. \tag{36}$$

Incorporating the relationship $\tilde{y}^\kappa = \hat{\xi}_1^\top \tilde{\theta}^\kappa + y_v$ and accumulating both sides of (36) from T_s (defined in Lemma 1) to k, we derive

$$V^\kappa(k) - V^\kappa(T_s) \leq -\frac{\rho\varepsilon^2}{2\|m_\kappa\|_\infty^2} \sum_{\tau=T_s}^{k-1} |\hat{\xi}_1(\tau)^\top \tilde{\theta}^\kappa(\tau)|^2 + \frac{\rho\varepsilon^2}{2} \sum_{\tau=T_s}^{k-1} |y_v(\tau)|^2 \tag{37}$$

wherein the boundedness of $m_\kappa(\cdot)$ has been utilized. Two different scenarios require separate analysis: In the first scenario, if $\sigma(T_s) = \kappa$, then the error signal $e_1(k) = \hat{\xi}_1^\top(k)\tilde{\theta}^\kappa(k)$. By applying the inequalities (35) to (37), we arrive at

$$\frac{\rho\varepsilon^2}{2}\left(\frac{1}{\|m_\kappa\|_\infty^2} - \bar{c}_\varepsilon^2\right) \sum_{\tau=T_s}^{k-1} |e_1(\tau)|^2 \leq V^\kappa(T_s) \tag{38}$$

for all $\varepsilon \in (0, \bar{\varepsilon}_4)$. Utilizing (35), it is noted that $\bar{c}_\varepsilon^2$ diminishes monotonically as ε approaches zero. Consequently, there is a threshold $\bar{\varepsilon}_5$ such that, for all $\varepsilon \in (0, \bar{\varepsilon}_5)$, $\frac{1}{\|m_\kappa\|_\infty^2} - \bar{c}_\varepsilon^2 > 0$ holds true. Consequently, it follows that

$$\sum_{\tau=T_s}^{k-1} |e_1(\tau)|^2 \leq \frac{2\|m_\kappa\|_\infty^2}{\rho\varepsilon^2(1 - \|m_\kappa\|_\infty^2 \bar{c}_\varepsilon^2)} V^\kappa(T_s) < \infty \tag{39}$$

for all $k \geq T_s$ and for all $\varepsilon \in (0, \bar{\varepsilon}_5)$.

In the secondary scenario, where $\sigma(T_s) \neq \kappa$, we can similarly establish the existence of a sufficiently small constant $\bar{\varepsilon}_6 > 0$ such that

$$\sum_{\tau=T_s}^{k-1} |e_1(\tau)|^2 \leq \frac{1}{\rho_1 - \rho_2 \bar{c}_\varepsilon}(V^\kappa(T_s) + \rho_3\varepsilon^2) < \infty \tag{40}$$

for certain positive constants ρ_1, ρ_2 and ρ_3, and for $\varepsilon \in (0, \bar{\varepsilon}_6)$. In sum, the acquisition of $\sum_{\tau=T_s}^{k-1} |e_1(\tau)|^2 < \infty$ corroborates our demonstration of $e_1(\cdot) \in \mathcal{L}_2$.

Ultimately, we ascertain that the trajectories of the closed-loop system are bounded and $\lim_{k\to\infty} y(k) = 0$. Recalling the fact that the storage function $W_0(k)$ satisfies the dissipation inequality $\Delta W_0(k) \leq \gamma_0^2|\nu_0(k)|^2 - \|e_0(k)\|^2$, as established in Proposition 1. We accumulate both sides of this inequality along the trajectories of systems Σ_0-Σ_3 over the time interval $[T_s, k)$. By invoking the results from Proposition 2 and Proposition 3 which state

$$\sum_{s=T_s}^{k-1} \|e_j(s)\|^2 \leq \varepsilon^2\gamma_j^2 \sum_{s=T_s}^{k-1} \|e_0(s)\|^2, \quad j = 2, 3,$$

we deduce that

$$W_0(k, \hat{\zeta}^\sigma(k)) < W_0(T_s, \hat{\zeta}^\sigma(T_s)) + 3\gamma_0^2|e_1(s)|^2 - (1 - 3\varepsilon^2\gamma_0^2(\gamma_2^2 + \gamma_3^2)) \sum_{s=T_s}^{k-1} \|e_0(s)\|^2.$$

Utilizing Lemma 1, along with the small-gain theorem, and defining $\bar{\varepsilon} := \min\{\bar{\varepsilon}_4, \bar{\varepsilon}_5, \bar{\varepsilon}_6, \frac{\sqrt{3}}{3\gamma_0(\gamma_2+\gamma_3)}\}$, we have

$$\|\hat{\zeta}^\sigma(k)\| \leq \sqrt{\frac{\varepsilon}{2\underline{c}_e}} \max\{\sqrt{\frac{2\bar{c}_e}{\varepsilon}}\|\hat{\zeta}^\sigma(T_s)\|, \sqrt{3}\gamma_0(\sum_{s=T_s}^{k-1} |e_1(s)|^2)^{\frac{1}{2}}\}$$

for all $k \in [T_s, +\infty)$ and $\varepsilon \in (0, \bar{\varepsilon})$, thus confirming that $\hat{\zeta}(\cdot) \in \mathcal{L}_\infty$. Given that $\hat{\theta}^\sigma(\cdot)$ is bounded within Θ^{N+1}, we deduce that $e_0(\cdot) \in \mathcal{L}_\infty$. The exponential stability of systems Σ_0, Σ_2 and Σ_3 further guarantees that all remaining state trajectories also belong to $\mathcal{L}_\infty$.

The established fact that $e_0(\cdot) \in \mathcal{L}_2$ leads to $\hat{\xi}_1(k) \in \mathcal{L}_\infty$ and $\Delta\hat{\xi}_1(k) \in \mathcal{L}_\infty$ for all $\varepsilon \in (0, \bar{\varepsilon})$. Correspondingly, $\hat{\theta}(k) \in \mathcal{L}_\infty$ and $\Delta\hat{\theta}(k) \in \mathcal{L}_\infty$. It is therefore deduced that $e_1(\cdot) \in \mathcal{L}_2 \cap \mathcal{L}_\infty$, $\Delta e_1(k) \in \mathcal{L}_\infty$ and $\lim_{k\to\infty} e_1(k) = 0$. Given that subsystems Σ_0, Σ_2 and Σ_3 exhibit exponential stability for all $\varepsilon \in (0, \bar{\varepsilon})$, it follows that $\hat{\zeta}(k)$, $\xi_2(k)$, $\xi_3(k)$, $\xi_a(k)$ and $z(k)$ all asymptotically converge to zero, leading to $\lim_{k\to\infty} y(k) = 0$. This completes the proof of Theorem 1. □

VI. Experimental results

A. Numerical Example

A simulation study is carried out to verify the effectiveness of the proposed approach. The plant model, characterized by a stable but non-minimum phase system

$$H(z) = \frac{z - 1.1}{z^2 - 1.4z + 0.69}. \tag{41}$$

The disturbance impacting the system is denoted by $d(k) = 1 + 2\sin(\omega_1 k) + 3\sin(\omega_2 k)$, with $\omega_1 = 0.2$ rad/s and $\omega_2 = 0.05$ rad/s, incorporating two distinct frequencies of excitation along with a bias term. The sampling time T is chosen as 0.01 s. The vector $\hat{v}$ in system (4) is belong to $\mathbb{R}^5$, and S $\mathrm{diag}(S_0, S_1, S_2)$, where $S_0 = 1$, $S_1 = \begin{pmatrix} \cos 0.2 & \sin 0.2 \\ -\sin 0.2 & \cos 0.2 \end{pmatrix}$ and $S_2 = \begin{pmatrix} \cos 0.05 & \sin 0.05 \\ -\sin 0.05 & \cos 0.05 \end{pmatrix}$. Table I summarizes the frequency response parameter, θ_i, $i = 0, 1, 2$, corresponding to different disturbances and their associated convex sets Θ_i, $i = 0, 1, 2$ in Fig. 4.

TABLE I
Parameter Vector and Subregions of the Parameter Set

Frequency	Ture parameter vector	Convex set
DC	$\theta_0 = -1.5385$	Θ_2
$\omega_1 = 0.2\,\mathrm{rad/s}$	$\theta_{1,1} = 1.3574$, $\theta_{1,2} = -3.1188$	Θ_3
$\omega_2 = 0.05\,\mathrm{rad/s}$	$\theta_{2,1} = -1.3375$, $\theta_{2,2} = -1.1037$	Θ_2

The parameters for the controller are selected as follows: $\varepsilon = 0.02$, $\beta = 1$, $\rho = 0.5$, $h = 0.7$, $r_1 = 0.1$, and $r_2 = 5$. All states of the closed-loop system are simulated starting from zero initial conditions, except for the parameter estimates $\hat{\theta}$, whose initial conditions are determined as follows

$$\hat{\theta}_i^j(0) = \begin{cases} (1,1)^\top, & \text{if } j = 1 \\ (-1,0)^\top, & \text{if } j = 2 \\ (1,-1)^\top, & \text{if } j = 3, \quad i \in \mathcal{N} \end{cases} \tag{42}$$

$$\hat{\theta}_0^j(0) = \begin{cases} 1, & \text{if } j = 1 \\ -1, & \text{if } j = 2. \end{cases} \tag{43}$$

In this scenario, each excitation frequency disturbance corresponds to 3 estimators (for the DC term in the disturbance,

there are 2 estimators), one of the three or two estimators is randomly selected as the initial index σ_i, $i \in \{0, 1, 2\}$.

Case 1. Applying the proposed controller, the simulation results are depicted in Fig. 7. The figure illustrates the time trajectories of $u-d$ and the closed-loop system output y, as well as the switching trajectory of the multi-model controller. It can be observed that the disparity between the control input u and disturbance d, and the plant output y, eventually converge to zero, indicating complete suppression of the disturbance. Additionally, the figure demonstrates that the switching of the multi-model controller stops within 3 seconds. Eventually, the estimates of the three disturbance frequencies all converge to convex sets that include the true parameter values, specifically $\sigma_0 = 2$, $\sigma_1 = 3$, and $\sigma_2 = 2$.

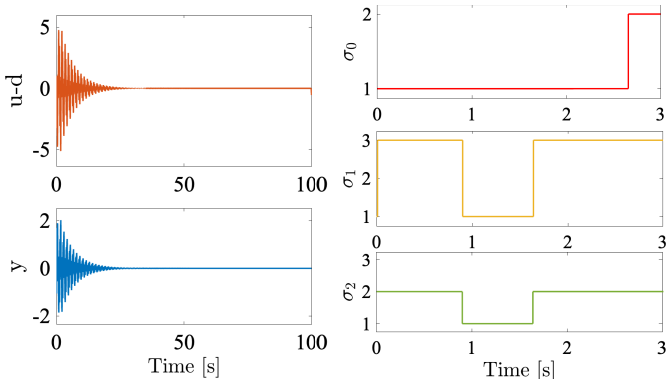

Fig. 7. Comparison of the time history of compensator error $\boldsymbol{u-d}$, plant output $\boldsymbol{y}$, and multi-controller index $\boldsymbol{\sigma_i}$ for $\boldsymbol{i \in \{0,1,2\}}$.

Case 2. Additionally, we verified the controller's robustness to disturbances of different frequencies. As illustrated in Fig. 8, building upon the Case 1 experiment, at 100 seconds, the disturbance d was switched to $2 + 2\cos(0.23k)$. The frequency of the new periodic disturbance term is 0.23 rad/s, with the corresponding frequency response parameter $\theta = (2.0993, -3.0835)^\top$. This parameter falls within the convex set Θ_3. It is evident that the output still converges to zero without requiring changes to the controller's parameter settings during runtime. We also demonstrate the robustness of the proposed algorithm by analyzing the impact of noisy output measurement (polluted by additive Gaussian noise with zero mean and 0.02 variance). This result suggests that the proposed controller is not sensitive to output measurement noise.

Overall, the simulation results validate the effectiveness of the proposed method in suppressing composite frequency disturbances with DC offsets, especially when the disturbance frequency decreases, demonstrating the over-parameterization capability of the controller.

B. ANC Experimental Results

To validate the effectiveness of the proposed controller in real-world application, a testing platform for ANC was constructed, as referenced in [22]. Fig. 9 displays the real test bench utilized in the facilities, showcasing important sections and depicting the hardware specifications of the experimental

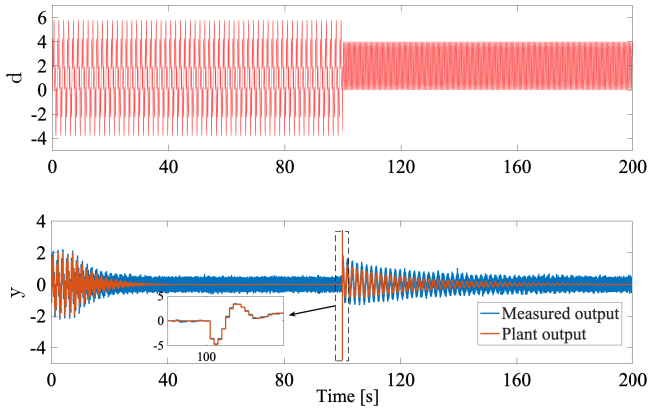

Fig. 8. Trajectories of the disturbance $\boldsymbol{d}$ and the plant output $\boldsymbol{y}$ under frequency switching.

platform: noise loudspeaker, anti-noise loudspeaker, measured output's microphone and computing device. Through this platform, experiments were conducted in a model-free system, demonstrating the capability of the proposed control algorithm in real acoustic environments. Fig. 10 displays the key components of ANC in a schematic representation. Both disturbance and controller's speakers are connected to a computer with NI Linux Real-Time operating environment. The system's measured output is denoted as $y(k)$, the control signal is indicated as $u(k)$, and the disturbance is denoted as $d(k)$.

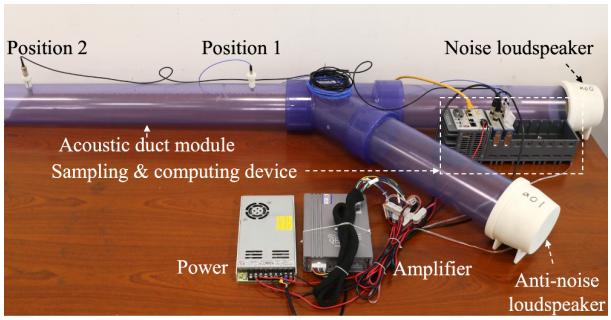

Fig. 9. Acoustic duct ANC test bench (photograph).

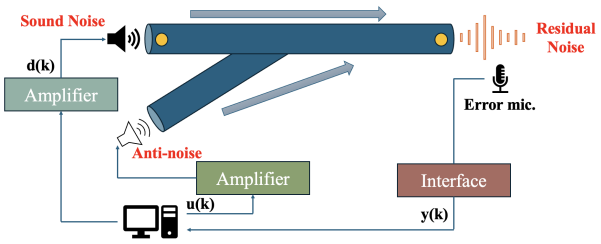

Fig. 10. Acoustic duct ANC test bench diagram.

Due to the relaxation of prior knowledge in our algorithm, even if the acoustic duct system is a model-free system, we only need to utilize the output signal collected from a single microphone, without requiring any additional reference signal.

Case 1. As illustrated in Fig. 11, the experimental setup initially operated in an open-loop mode for 5 seconds (with the control signal $u(k) = 0$). During this time, noise interference with frequencies of 279 Hz and 317 Hz was introduced, as depicted in Fig. 12. At the 5-second mark, the controller is activated, and a multi-model controller was employed to suppress the interference. The controller parameters were set as follows: $\varepsilon = 0.02$, $\beta = 1$, $\rho = 0.5$, $h = 0.7$, $r_1 = 0.1$ and $r_2 = 3$. The sampling time T is chosen as 0.2 ms. Fig. 11 illustrates the performance of the controller in suppressing the interference, achieving a decay of nearly -30 dB. Furthermore, once the system was closed, the adaptive controller swiftly transitioned to the correct index. However, as shown in Fig. 12, additional high-frequency components and noise were present in the spectral output of the speaker due to factors such as environmental echoes, reflections, and nonlinear responses in the speaker. Nonetheless, noise at the excitation frequency was entirely suppressed.

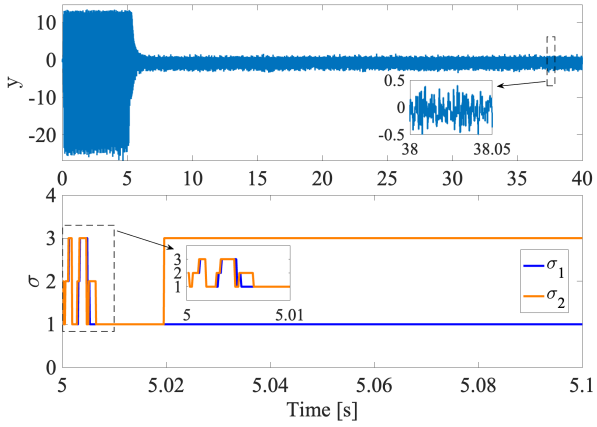

Fig. 11. Composite frequency noise cancellation performance in the time domain and the time trajectory of the switching signal, with a close-up view highlighting the rapid switching during transients.

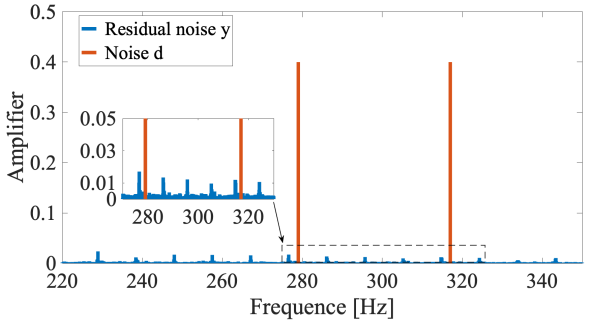

Fig. 12. A comparison of the spectra of the disturbance $\boldsymbol{d}$ and the noise-cancelled system output $\boldsymbol{y}$.

Case 2. In this experiment, we challenged our algorithm by suddenly changing the position of the error microphone. Specifically, we conducted two-frequency noise cancellation experiments, relocating the microphone from position 1 to position 2. The results of these experiments are illustrated in Fig. 13. The results indicate that the achieved suppression remained consistent before and after the relocation. Meanwhile, it can be observed that due to system variation, the frequency response parameters of the system also changed. The parameter estimates, which had stabilized after Case 1, were further updated to new estimates. This suggests that even without prior knowledge of the system model, the parameter estimator can automatically update to values near the true parameters. Thus, the controller proposed in this paper exhibits robust adaptability in unknown 3D environments, regardless of the specific error microphone configurations.

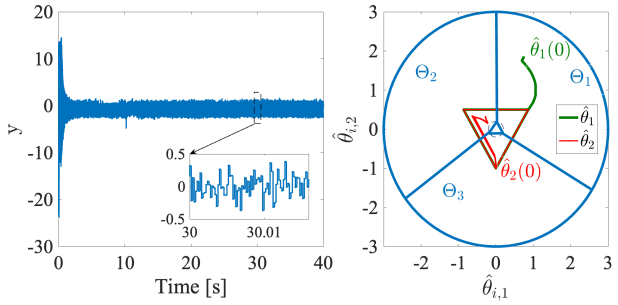

Fig. 13. Trajectories of the system output $\boldsymbol{y}$ and the parameter estimation $\hat{\boldsymbol{\theta}}$, $\boldsymbol{i} \in \{\mathbf{1}, \mathbf{2}\}$ at the microphone position 2.

VII. Conclusion

In this study, we introduce an innovative AFC-based approach that obviates the need for the SPR-like condition for uncertain discrete-time systems influenced by a biased multi-sinusoidal. Stability analyses affirm that the system's output asymptotically approaches zero. The numerical example and experimental results compellingly showcase the system's adeptness at rejecting unwanted noise, without relying on a predefined system model. Future endeavors will focus on broadening these findings to encompass the scenario of unknown frequency sinusoids within MIMO uncertain systems, while exploring a broader range of practical application.

References

[1] M. Ramírez-Neria, J. Morales-Valdez, and W. Yu, "Active vibration control of building structure using active disturbance rejection control," *Journal of Vibration and Control*, vol. 28, no. 17-18, pp. 2171–2186, 2022.

[2] Z. Chen and J. Huang, "Attitude tracking of rigid spacecraft subject to disturbances of unknown frequencies," *International Journal of Robust and Nonlinear Control*, vol. 24, no. 16, pp. 2231–2242, 2014.

[3] C. Kang and T.-C. Tsao, "Control of magnetic bearings for rotor unbalance with plug-in time-varying resonators," *Journal of dynamic systems, measurement, and control*, vol. 138, no. 1, p. 011001, 2016.

[4] M. Bodson, J. S. Jensen, and S. C. Douglas, "Active noise control for periodic disturbances," *IEEE Transactions on control systems technology*, vol. 9, no. 1, pp. 200–205, 2001.

[5] I. D. Landau, R. Meléndez, L. Dugard, and G. Buche, "Robust and adaptive feedback noise attenuation in ducts," *IEEE Transactions on Control Systems Technology*, vol. 27, no. 2, pp. 872–879, 2019.

[6] B. Francis and W. Wonham, "The internal model principle of control theory," *Automatica*, vol. 12, no. 5, pp. 457–465, 1976.

[7] V. Nikiforov and D. Gerasimov, *Adaptive regulation: reference tracking and disturbance rejection*, vol. 491. Springer Nature, 2022.

[8] S. Jafari and P. A. Ioannou, "Robust adaptive attenuation of unknown periodic disturbances in uncertain multi-input multi-output systems," *Automatica*, vol. 70, pp. 32–42, 2016.

[9] R. Marino and P. Tomei, "Adaptive disturbance rejection for unknown stable linear systems," *Transactions of the Institute of Measurement and Control*, vol. 38, no. 6, pp. 640–647, 2016.

[10] P. Tomei and R. Marino, "Adaptive regulation for minimum phase systems with unknown relative degree and uncertain exosystems," *Automatica*, vol. 147, p. 110678, 2023.

[11] Y. Wang, G. Pin, A. Serrani, and T. Parisini, "Removing spr-like conditions in adaptive feedforward control of uncertain systems," *IEEE Transactions on Automatic Control*, vol. 65, no. 6, pp. 2309–2324, 2020.

[12] M. Kamaldar and J. B. Hoagg, "Adaptive harmonic control for rejection of sinusoidal disturbances acting on an unknown system," *IEEE Transactions on Control Systems Technology.*, vol. 28, no. 2, pp. 277–290, 2020.

[13] M. Bin, L. Marconi, and A. R. Teel, "Adaptive output regulation for linear systems via discrete-time identifiers," *Automatica*, vol. 105, pp. 422–432, 2019.

[14] P. Tomei, "Multi-sinusoidal disturbance rejection for discrete-time uncertain stable systems," *Automatica*, vol. 79, pp. 144–151, 2017.

[15] J. Huang, *Nonlinear Output Regulation*. Society for Industrial and Applied Mathematics, 2004.

[16] A. Krolikowski and D. Horla, "Discrete-time adaptive internal model control," in *International Conference on Circuits, Systems, Signals*, pp. 112–115, 2008.

[17] M. T. Shahab and D. E. Miller, "Adaptive control of a class of discrete-time nonlinear systems yielding linear-like behavior," *Automatica*, vol. 130, p. 109691, 2021.

[18] S. Pedone and A. Fagiolini, "Robust discrete-time lateral control of racecars by unknown input observers," *IEEE Transactions on Control Systems Technology*, vol. 31, no. 3, pp. 1418–1426, 2023.

[19] J. Chandrasekar, L. Liu, D. Patt, P. Friedmann, and D. Bernstein, "Adaptive harmonic steady-state control for disturbance rejection," *IEEE Transactions on Control Systems Technology.*, vol. 14, no. 6, pp. 993–1007, 2006.

[20] M. Kamaldar and J. B. Hoagg, "Time-domain adaptive harmonic control for rejection of sinusoidal disturbances acting on an unknown discrete-time system," in *2017 American Control Conference (ACC)*, pp. 5690–5695, 2017.

[21] Y. Yan and J. Huang, "Robust output regulation problem for discrete-time linear systems with both input and communication delays," *Journal of Systems Science and Complexity*, vol. 30, pp. 68–85, 2017.

[22] I. Doré Landau, M. Alma, A. Constantinescu, J. J. Martinez, and M. Noë, "Adaptive regulation—rejection of unknown multiple narrow band disturbances (a review on algorithms and applications)," *Control Engineering Practice*, vol. 19, no. 10, pp. 1168–1181, 2011.

[23] X. Guo and M. Bodson, "Analysis and implementation of an adaptive algorithm for the rejection of multiple sinusoidal disturbances," *IEEE Transactions on Control Systems Technology*, vol. 17, no. 1, pp. 40–50, 2009.

[24] S. Aranovskiy and L. B. Freidovich, "Adaptive compensation of disturbances formed as sums of sinusoidal signals with application to an active vibration control benchmark," *European Journal of Control*, vol. 19, no. 4, pp. 253–265, 2013.

[25] R. A. de Callafon and H. Fang, "Adaptive regulation via weighted robust estimation and automatic controller tuning," *European Journal of Control*, vol. 19, no. 4, pp. 266–278, 2013.

[26] S. Jafari, P. Ioannou, B. Fitzpatrick, and Y. Wang, "Robustness and performance of adaptive suppression of unknown periodic disturbances," *IEEE Transactions on Automatic Control*, vol. 60, no. 8, pp. 2166–2171, 2015.

[27] J. B. Hoagg, M. A. Santillo, and D. S. Bernstein, "Discrete-time adaptive command following and disturbance rejection with unknown exogenous dynamics," *IEEE Transactions on Automatic Control*, vol. 53, no. 4, pp. 912–928, 2008.

[28] R. Chi, Y. Hui, B. Huang, and Z. Hou, "Active disturbance rejection control for nonaffined globally lipschitz nonlinear discrete-time systems," *IEEE Transactions on Automatic Control*, vol. 66, no. 12, pp. 5955–5967, 2021.

[29] Z. Hou, R. Chi, and H. Gao, "An overview of dynamic-linearization-based data-driven control and applications," *IEEE Transactions on Industrial Electronics*, vol. 64, no. 5, pp. 4076–4090, 2017.

[30] G. Yang, J. Yao, and Z. Dong, "Neuroadaptive learning algorithm for constrained nonlinear systems with disturbance rejection," *International Journal of Robust and Nonlinear Control*, vol. 32, no. 10, pp. 6127–6147, 2022.

[31] C. Chen, L. Xie, Y. Jiang, K. Xie, and S. Xie, "Robust output regulation and reinforcement learning-based output tracking design for unknown linear discrete-time systems," *IEEE Transactions on Automatic Control*, vol. 68, no. 4, pp. 2391–2398, 2023.

[32] J. Zhao, C. Yang, W. Gao, and J. H. Park, "Incremental reinforcement learning and optimal output regulation under unmeasurable disturbances," *Automatica*, vol. 160, p. 111468, 2024.

[33] Y. Ren, Q. Wang, and Z. Duan, "Output-feedback q-learning for discrete-time linear h∞ tracking control: A stackelberg game approach," *International Journal of Robust and Nonlinear Control*, vol. 32, 05 2022.

[34] G. Dulac-Arnold, N. Levine, D. J. Mankowitz, J. Li, C. Paduraru, S. Gowal, and T. Hester, "Challenges of real-world reinforcement learning: definitions, benchmarks and analysis," *Machine Learning*, vol. 110, no. 9, pp. 2419–2468, 2021.

[35] W. Chu, "Abel's lemma on summation by parts and basic hypergeometric series," *Advances in Applied Mathematics*, vol. 39, no. 4, pp. 490–514, 2007.

[36] J. Xu, S. Liu, J. Jia, and Y. Wang, "Robust output regulation for uncertain discrete-time linear systems under the effect of a sinusoidal disturbance," *IFAC-PapersOnLine*, vol. 56, no. 2, pp. 2895–2902, 2023.

Jiangkun Xu received the B.S. degree in Electronic Information Engineering from Northwest University, China, in 2021. He is working toward the Master degree majoring in Information and Communication Engineering at School of Information Science and Technology, ShanghaiTech University, Shanghai, China. His research interests include output regulation and discrete-time systems.

Yizhou Gong received the B.S. degree in automation from North China Electric Power University, China, in 2022. He is working toward the Ph.D. degree majoring in electrical and electronic engineering at School of Information Science and Technology, ShanghaiTech University, Shanghai, China. His research interests include adaptive control, output regulation and observer design.

Yang Wang received her B.Eng. degree in Electrical and Electronic Engineering from Tongji University, Shanghai, China, in 2013, and her M.Sc. and Ph.D. degrees in Control Systems from Imperial College London, U.K., in 2014 and 2019, respectively. From 2014 to 2019, she held visiting scholar positions at the University of Cambridge, U.K., and Ohio State University, Ohio, USA. Since 2020, she has been an Assistant Professor at the School of Information Science and Technology, ShanghaiTech University, Shanghai, China. Her work has been supported by the Yangfan Program of STCSM, Shanghai. Her research interests lie at the intersection of nonlinear and adaptive control theory, with applications in fluidic systems, robotics, and automotive engineering.